PeV Photon and Neutrino Flares from Galactic Gamma-Ray Binaries

A. M. Bykov[1] , A. E. Petrov[1] , M. E. Kalyashova[1,2] , and S. V. Troitsky[3]
[1] Ioffe Institute, 26 Politechnicheskaya, St. Petersburg, 194021, Russia
[2] Peter the Great St. Petersburg Polytechnic University, 29 Politechnicheskaya, St. Petersburg, 195251, Russia
[3] Institute for Nuclear Research of the Russian Academy of Sciences, 60th October Anniversary Prospect 7a, Moscow, 117312, Russia

Abstract

The high-energy radiation from short period binaries containing a massive star with a compact relativistic companion was detected from radio to TeV γ-rays. We show here that PeV regime protons can be efficiently accelerated in the regions of collision of relativistic outflows of a compact object with stellar winds in these systems. The accelerated proton spectra in the presented Monte Carlo model have an upturn in the PeV regime and can provide very hard spectra of sub-PeV photons and neutrinos by photomeson processes in the stellar radiation field. The recent report of a possible sub-PeV γ-ray flare in coincidence with a high-energy neutrino can be understood in the frame of this model. The γ-ray binaries may contribute substantially to the Galactic component of the detected high-energy neutrino flux.

Unified Astronomy Thesaurus concepts: High-energy cosmic radiation (731); Gamma-ray sources (633)

1. Introduction

The cosmic accelerators of petaelectronovolt (PeV) energy particles revealed themselves through the measured fluxes of the Galactic cosmic rays as well as by the high-energy neutrinos first detected by IceCube (Aartsen et al. 2013; IceCube Collaboration 2013). Ground-based γ-ray telescopes found a population of sources with power-law spectra extending above 10 TeV without a clear signature of the spectral cutoff (HESS Collaboration et al. 2016; Aharonian et al. 2019), which can be associated with cosmic pevatrons. Strong attenuation of γ-ray fluxes above 100 TeV due to photon–photon pair production limits the possibility of the γ-ray pevatron detection mainly to a population of nearby Galactic sources at distance $D \lesssim 10$ kpc (Nikishov 1962; Dermer & Menon 2009). The Large High Altitude Air Shower Observatory (LHAASO) collaboration reported a significant detection of 12 γ-ray sources above 100 TeV and up to 1.4 PeV highlighting the problem of the origin of these PeV accelerators (Cao et al. 2021a). The Carpet-2 experiment team (Dzhappuev et al. 2021) recently reported the detection of a 3.1σ excess of γ-ray flux above 300 TeV from the Cygnus region associated with a 150 TeV neutrino event detected by IceCube (IceCube Collaboration 2020) and most likely consistent with a flare of a few months duration. The γ-ray energy flux during the flare is $\gtrsim 10^{-9}$ erg cm^{-2} s^{-1}, an order of magnitude higher than the 95% CL upper limit on the steady-state flux, $\lesssim 1.2 \times 10^{-10}$ erg cm^{-2} s^{-1}, obtained for the same source by Carpet-2. The flare flux is well above the fluxes in the TeV regime detected from the population of γ-ray sources in the region (see, e.g., Amenomori et al. 2021). It also highly exceeds the fluxes from known γ-ray sources including the γ-ray pulsars, supernova remnants (e.g., Tibet ASγ Collaboration et al. 2021), superbubbles (e.g., Abeysekara et al. 2021), and γ-ray binaries (e.g., Aharonian et al. 2006) as well as from unidentified PeV candidate sources (e.g., Abdalla et al. 2021; Cao et al. 2021b).

Most high-energy neutrinos are probably extragalactic. Combined IceCube and ANTARES data (Albert et al. 2018) limit the Galactic contribution to $\lesssim 15\%$, and the first indications of the presence of this component have been found (Aartsen et al. 2019). Some Galactic contribution helps to naturally explain (Palladino & Vissani 2016) the tension between different measurements of the neutrino spectrum, see, e.g., Abbasi et al. (2021). For a review of particular classes of Galactic sources, see Kheirandish (2020). Gamma-ray binaries were proposed as high-energy neutrino sources long ago (see, e.g., Levinson & Waxman 2001; Distefano et al. 2002; Bednarek 2005; Sahakyan et al. 2014).

The angular resolution of both Carpet-2 and IceCube does not allow one to identify a particular source of the photon flare and of the contemporaneous neutrino in the densely populated Cygnus region. The time variability on a timescale of a few months and the high observed γ-ray flux make any associations of the source with extended supernova remnants or superbubbles very unlikely. A number of compact Galactic sources of high-energy radiation are located in the Cygnus region, including γ-ray binaries Cyg X-3 and PSR J2032+4127.

The maximum energies of protons accelerated by outflows with frozen-in magnetic fields of a kinetic/magnetic luminosity $\mathcal{L}_K$ can be estimated from the equation:

$$E_{\max} \approx \frac{f(\beta_{\mathrm{f}})}{\Gamma_{\mathrm{f}} \Omega} \left(\frac{\mathcal{L}_K}{5 \times 10^{34} \text{ erg s}^{-1}} \right)^{1/2} \text{PeV}, \quad (1)$$

where the dimensionless velocity of the flow is $\beta_{\mathrm{f}} = u_f/c$, c is the speed of light, $\Gamma_{\mathrm{f}} = 1/\sqrt{1 - \beta_{\mathrm{f}}^2}$, and Ω is the opening angle of the outflow (see, e.g., Lemoine & Waxman 2009; Bykov et al. 2012, and references therein). The function $f(\beta_{\mathrm{f}}) \propto \beta_{\mathrm{f}}^{1/2}$ for $\beta_{\mathrm{f}} \ll 1$, while $f(\beta_{\mathrm{f}}) \sim 1$ for ultrarelativistic flow with $\Gamma_{\mathrm{f}} \gg 1$. It follows from the equation that for a given $\mathcal{L}_K$, the higher values of $E_{\max}$ can be achieved for the mildly relativistic flows with $\beta_{\mathrm{f}} \Gamma_{\mathrm{f}} \sim 1$ with relatively narrow opening angle $\Omega < 1$. Then $\mathcal{L}_K > 3 \times 10^{35}$ erg s^{-1} and $\Omega < 1/3$ are needed to reach the energy of the accelerated proton ~ 10 PeV.

Equation (1) does not account for radiative losses, which can reduce $E_{\max}$ substantially.

The observed flare flux transforms to the γ-ray luminosity above 300 TeV of $L_\gamma \sim 4 \times 10^{35}(D/1.5 \text{ kpc})^2 \text{ erg s}^{-1}$. Thus, if the source is indeed located in the Cygnus star-forming region, then, according to Equation (1), the $\mathcal{L}_K$ required to produce PeV regime particles radiating 300 TeV photons is comparable to L_γ.

One can conclude that a very hard spectrum of accelerated particles and a fast cooling of PeV particles are needed in order for the required kinetic/magnetic luminosity to be consistent with that available in compact relativistic sources of stellar masses. We present below a model of the compact γ-ray sources that can convert a substantial fraction of their kinetic luminosity (provided by the magnetic braking of a pulsar, magnetic field reconnection in a magnetar, or accretion onto a black hole) to the PeV regime γ-rays and neutrinos by the photomeson production mechanism in proton–photon collisions. Gamma-ray binary sources (LS 5039, PSR B1259-63, LSI $+61°$ 303, PSR J2032+4127, and others, see, e.g., Dubus 2013) can be considered as possible candidates. Well-known powerful microquasar Cyg X-3 demonstrated giant γ-ray flares (Corbel et al. 2012). In all of these sources, which have been subjects of extensive modeling for a long time (see, e.g., Tavani & Arons 1997), the compact object has a massive early-type star companion.

The model of a PeV source we discuss here suggests the interaction of a fast outflow from a compact relativistic object with the stellar wind (SW) of a bright massive star. The colliding magnetized flows provide a plausible site of fast Fermi-type acceleration of TeV-energy particles preaccelerated in the vicinity of the compact object up to PeV regime. The acceleration mechanism at the colliding wind flows (CWFs) may form a very hard spectrum of particles in the TeV–PeV energy range. In addition to γ-ray radiation produced in proton–proton collisions, the accelerated PeV protons interact efficiently with the optical photons of the luminous massive star by the photomeson mechanism providing fast cooling in PeV γ-rays and neutrinos. In the next section we will discuss the PeV γ-ray and neutrino production in the generic source PSR J2032+4127; though, a similar model could be applied to other binary sources including either pulsar winds (PWs) or jets of the accreting black holes.

2. Model

PSR J2032+4127 is located at a distance of ~ 1.4 kpc and orbits around a massive Be star MT91 213 (B0Vp) with a long period of ~ 50 yr (Ho et al. 2017). Its spin-down power $\dot{E}$ may reach $3 \times 10^{35} \text{ erg s}^{-1}$ (Camilo et al. 2009). This is close to the γ-ray luminosity $\sim 2.7 \times 10^{35} \text{ erg s}^{-1}$ at the lower limit of the Carpet-2 measurement uncertainty band. This suggests that most of the CWF acceleration source power should be converted into PeV-range proton energy. The total available power of the CWF is a sum of the pulsar spin-down power and the fraction of the SW power released in the CWFs. Fermi I type acceleration in the CWFs can produce particle energy distribution $f(E) \propto E^{-s}$ with $s \sim 1$, where energy is mainly accumulated by the most energetic particles (see Bykov et al. 2017). Efficient acceleration at CWFs may be caused by the passage of the pulsar through the equatorial region of the Be star SW. In November 2020 the pulsar was at ~ 20 au from MT91 213, which is about ~ 400 stellar radii allowing the
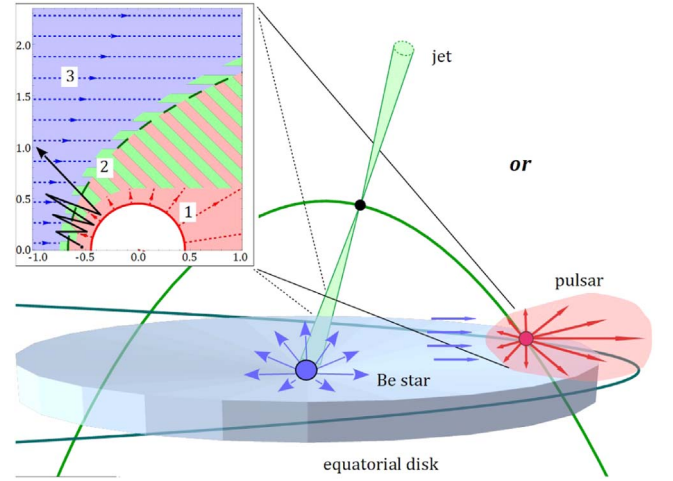
Figure 1. Sketch of the interaction of mildly relativistic flows produced by a compact object (pulsar or black hole) with the equatorial disk of a Be star. Inset: spatial structure of the Monte Carlo model diffusion zones. (1) Pink: shocked pulsar wind. (2) Cross-hatched with green: zone around the contact discontinuity (approximate position—dashed green line). (3) Blue: stellar wind. The white zone is the cold pulsar wind. The red solid line shows the termination shock of the pulsar wind, dashed lines with arrows are the directions of flows. Lengths are normalized to 2.5×10^{14} cm. The black imposed polygonal line illustrates a trajectory of a particle accelerated in the colliding flows.

interaction of the PW with the Be star equatorial disk (Klement et al. 2017).

The model of PeV flares of PSR J2032+4127 we discuss here uses only the hadronic emission processes. Severe synchrotron radiation losses do not allow acceleration of PW leptons to PeV energies at the considered orbital phase. The toroidal SW magnetic field component scaling $\propto r^{-1}$ gives ~ 1 G at a distance of $r \sim 20$ au, if the surface dipolar stellar field is ~ 1 kG. For a fast rotating star with mass $M_* \sim 15 M_\odot$ and radius $R_* \sim 10 R_\odot$, an even higher field of ~ 2 kG may be expected (see, e.g., Shultz et al. 2019).

We simulate acceleration at the CWFs using the kinetic Monte Carlo model described in Section 4 of Bykov et al. (2017) adapted for this problem. This model allows simulation of the diffusive particle propagation in the region where the PW collides with the ambient matter flow, launching the PW termination shock and possibly the bow shock. The model plausibly catches the spatial structure of CWF system represented by spatial zones with reasonable parameters of diffusion and magnetic fields and includes a simple model of flow velocity distribution (see Figure 1).

Protons are injected in the CWF region with a wide soft power-law spectrum $f_{\text{inj}}(E) \propto E^{-s}$ with $s \sim 2.2$ (e.g., Sironi et al. 2015; Amato 2019). It is produced by Fermi I type acceleration at the termination shock formed in the collision of the pair-dominated pulsar wind with magnetized plasma of stellar wind. Both pairs and protons have to be accelerated in this system. In the simulation we generate a population of particles with the energy distribution function $f_{\text{inj}}(E)$ and inject them in the CWFs at the contact discontinuity (see Figure 1).

Particles then propagate through the CWFs according to the adopted diffusion model. The diffusion coefficients are chosen in the Bohm limit, i.e., defined by the particle energy and local magnetic field. Each particle propagates to a distance defined by its mean free path (mfp) given by the diffusion coefficient at its location, then it is scattered isotropically in the local plasma

rest frame, and then again propagates to an mfp distance, and so on, until it leaves the simulation. All the generated particles are propagated through the simulation area one by one. Multiple subsequent scatterings and crossings of the contact discontinuity in the zone of almost head-on wind collision allows particles to gain energy. Particles can be accelerated until either their mfp exceeds the size of the accelerator allowing them to escape through the border with the free escape boundary condition, or they lose too much energy due to adiabatic and radiative losses and therefore join the low-energy particle pool.

Relativistic protons radiate mainly due to interactions with stellar photons (the photomeson process, also dubbed "$p\gamma$") and SW protons (pp process). The radiative losses (including synchrotron and inverse Compton) are accounted for at each scattering by subtraction of the energy radiated by a particle in all the radiation processes during the preceding free propagation flight. We calculate the radiation loss rates using the approach of Kafexhiu et al. (2014) for the pp process and the approach of Kelner & Aharonian (2008) for the $p\gamma$ process.

Detection of momenta of all particles leaving the simulation box with the Monte Carlo techniques allows us to obtain the spectral energy distribution of particles accelerated by the CWFs, averaged over the simulation volume. Then, the emission produced in $p\gamma$ and pp processes is calculated using parameterizations of Kelner & Aharonian (2008) and Kafexhiu et al. (2014). We take into account the finite size of the simulation box, scaling the photon field $\propto r^{-2}$ with distance from the star r. To do so, we divide the box into a number of spatial bins, calculate the emission flux produced by each bin separately, and finally summarize the results.

For a thermal distribution of stellar photons with $T \approx 30,000\,K$, the $p\gamma$ process works above a threshold proton Lorentz-factor $\Gamma_p \gtrsim 10^7$ (e.g., Dermer & Menon 2009). Thus, to enable the $p\gamma$ process for the peak of a CWF-produced hard energy distribution, the peak should lie at $\gtrsim 10\,PeV$.

The structure of the outer disks of Be stars was studied by Klement et al. (2017). They estimated the outer disk extensions to be up to ∼400 equatorial radii of the star and found that the disk height H scales as $H \propto r^{3/2}$. This means that the disk could extend to the distance of about 20 au with the width well above 1 au.

The maximum standoff distance $R_{sd} = \sqrt{\dot{E}/4\pi\rho u^2 c} \sim 10$ au defining the CWF acceleration region size is limited by the orbital separation distance. Here ρ and u are the SW mass density and velocity at the wind interaction region. Confinement of a particle with a gyroradius r_g in the CWFs, $r_g \lesssim R_{sd}$, then requires the magnetic field $\gtrsim 1\,G$. For the surface dipolar field of the star ∼1 kG the toroidal SW field allows ∼2 G at $r \sim 2 \times 10^{14}$ cm.

At $r \gg R_*$ the radial component of SW velocity is its terminal velocity $v_\infty \sim \sqrt{2GM_*/R_*} \approx 800\,km\,s^{-1}$, where G is the gravitational constant. This is much faster than the orbital velocity of $v_K \sim 30\,km\,s^{-1}$ and the wind toroidal velocity of ∼a few km s^{-1}. Thus, we assume the SW velocity to be $u \approx v_\infty$ and the SW proton number density to be ∼3000 cm^{-3}, corresponding to the SW disk density at the stellar surface of $\sim 10^{-12}\,g\,cm^{-3}$ (Klement et al. 2017).

The timescale of the acceleration in the CWFs is much shorter than the flare duration of ∼10^7 s. According to Equation (21) from Bykov et al. (2017) it takes ∼10^6 s to produce a hard energy distribution peaking at tens of PeV. The
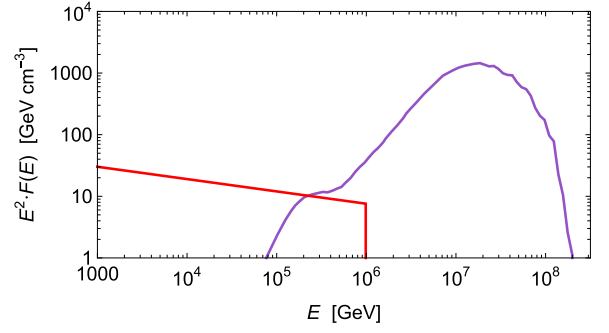
Figure 2. (Red) The energy distribution function of particles injected into the colliding wind flows (extends down to 1 GeV). (Purple) The result of the Monte Carlo simulation of the spectrum of particles accelerated in the colliding wind flows in the collision zone of the pulsar and stellar winds.
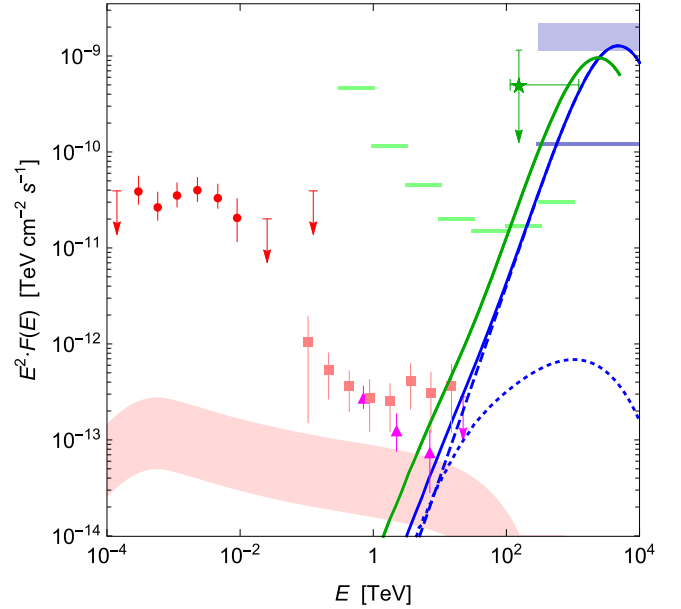
Figure 3. High-energy emissions from the source in the Cygnus region. Blue: photons from the total (full curve) simulated flare flux; contributions from p–p (dotted) and p–γ (dashed) interactions of protons accelerated in colliding winds. Red shaded area: photons from the p–p interaction of the injection spectrum protons (within the source parameter uncertainties). Violet shaded area: Carpet-2 flare flux. Magenta and pink data points: VERITAS and MAGIC steady-state fluxes (Abeysekara et al. 2018); red points in the GeV range are Fermi/LAT steady-state data (Chernyakova et al. 2020). Violet horizontal line: Carpet-2 95% CL upper limit on the steady-state flux. Green: neutrinos' estimated total flare flux (full curve); horizontal lines represent the 90% CL IceCube (IceCube Collaboration et al. 2021) upper limit on the steady-state neutrino flux of Cyg X-3, which is expected to be similar to that of PSR J2032 +4127. Star: an order-of-magnitude estimate (Dzhappuev et al. 2021) of the flare flux from the detection of one 150 TeV neutrino (IceCube Collaboration 2020).

CWF acceleration may provide a high enough value of γ-ray flux during the pulsar passage through the disk that also may take $H/u \sim 10^7$ s.

3. Results and Discussion

Figure 2 presents the simulated spectrum of accelerated protons. The red curve shows the injection spectrum, and the purple curve shows the particle spectrum after the CWF acceleration. The latter is much harder and peaks at a few tens of PeV, where most of the particle energy is accumulated.

In Figure 3 we show the simulated emission spectra produced by the modeled particle distribution. The pp γ-ray flux (dotted curve) is well below the Carpet-2 measured flux, whereas $p\gamma$ flux (dashed curve) produced by particles accelerated up to tens of PeV allows us to explain the results of Carpet-2 flare measurements. At TeV energies the total flux produced in both hadronic processes does not exceed even the steady-state fluxes observed by VERITAS and MAGIC (Abeysekara et al. 2018). The Fermi LAT 1–10 GeV lightcurve of PSR J2032+4127 is stable along the whole orbit with the flux $\sim 10^{-10}$ erg cm^{-2} s^{-1} (Chernyakova et al. 2020). It is likely produced by the pulsar magnetospheric emission and the flux is well above that from hadronic interactions described by our model, see Figure 3. The GeV–TeV spectra are successfully modeled within the leptonic scenario (see, e.g., Takata et al. 2017; Chernyakova et al. 2020). As was mentioned above, severe radiation losses exclude the leptonic origin of PeV γ-ray emission. Interestingly, the indications of lepton spectral break from $s \sim 2$ to a harder $s \sim 1$, similar to those shown in Figure 2 for the proton spectrum, were obtained in the hard X-ray spectrum of LS 5039 detected with IBIS INTEGRAL (Falanga et al. 2021).

The γ-ray binaries may represent a possible population of cosmic-ray sources with hard spectra. This can be important, e.g., to resolve the issues with energetics of high-energy radiation discussed by Murase & Fukugita (2019).

The effects of the absorption of GeV–TeV γ-rays in close γ-ray binaries containing luminous massive stars were discussed in the cases of LS 5039, LSI +61° 303, and Cyg X-3 (see, e.g., Cerutti et al. 2011). However, in the source considered above, the attenuation of PeV photons of interest due to e$^\pm$ pair production on the intensive stellar radiation is not essential.

The predicted neutrino flux is compared in Figure 3 with typical estimates of the flare and steady-state neutrino emission from IceCube data. Like in γ-rays, the flare neutrino flux is an order of magnitude higher than the steady one. The overall contribution of this and similar sources to the IceCube astrophysical neutrino flux is limited by short duty cycles and by a small number of sources. We estimate that the time-averaged flux from all γ-ray binaries can reach at most ($\sim$10%–13%) of the full-sky astrophysical neutrino flux, in agreement with constraints on the diffuse Galactic component (Albert et al. 2018); studies of point-source contributions (e.g., IceCube Collaboration et al. 2021) are less constraining.

In the PeV source model we considered a particular geometry of the mildly relativistic colliding flows of PW—the massive Be star wind shown in Figure 1. The same mechanism can rapidly accelerate the protons up to PeV energies in other γ-ray binaries, e.g., in the case of the black hole jet colliding with the massive star wind also illustrated in Figure 1. The realistic models of interaction of the fast outflow from a compact object with the wind of a massive star are still under debate. The models of microquasars like Cyg X-1 and Cyg X-3 with fast supersonic outflows (relativistic jets) due to accretion onto a black hole (see, e.g., Romero et al. 2017, and the references therein) represent a few of these. Apart from the microquasars and pulsar wind nebulae (e.g., Arons 2012; Amato 2019) the powerful outflows of the high enough kinetic luminosities (consistent with that given by Equation (1)) in supernova remnants (Cristofari 2021), compact stellar clusters (Bykov et al. 2015), and superbubbles can accelerate protons above PeV and produce (sub-)PeV γ-rays and neutrinos. The distinctive feature of the model of the γ-ray binary PSR J2032 +4127—MT91 213 discussed above is the combination of both the fast production of hard energy spectra of protons peaking in the PeV regime and the fast efficient photomeson cooling in the vicinity of the B0Vp star, which provides the highest PeV regime luminosity.

4. Conclusions

The model we discuss in the paper allows us to convert a sizable fraction of the kinetic power of the outflows of the compact objects in close binary systems into PeV regime radiation due to the high efficiency of the Fermi mechanism in colliding flows. Recent modeling by Pittard et al. (2021) of the TeV regime particle acceleration in the colliding wind binary with wind velocities of $\sim$a few $\times 10^3$ km s^{-1} and $\sim$mG magnetic fields in the acceleration region demonstrated that $\sim$30% of the wind power was transferred to nonthermal particles. In our model, with the short binary separation allowing for $\gtrsim G$ magnitude magnetic fields and mildly relativistic flows produced by shocked relativistic outflow of a compact object, one can reach a similarly high efficiency but for proton acceleration to the PeV energy regime. The rapid photomeson cooling of the PeV protons converts a significant part of the available kinetic power into (sub-)PeV photons and neutrinos.

Our model generally predicts a transient character of the very bright PeV regime radiation. The main reason for this is the presence of variations in the magnetic field, particle, and seed photon densities along the orbit of the compact object due to the disks (for a Be companion star) or anisotropic stellar winds. This provides variability of the very-high-energy radiation along the compact object orbit. The timescale to cross the Be star disk could be a few months for the orbital parameters of PSR J2032+4127, which may explain the estimated duration of the γ-ray flare detected by Carpet-2.

An important factor is also the threshold character of the photomeson radiation mechanism. Indeed, the energy of a seed photon in the rest frame of the accelerated proton must exceed $\sim$200 MeV to start the mechanism, which requires protons of energies above 10 PeV to interact with the intense optical radiation of the massive star.

A transient activation of the efficient and fast Fermi I type acceleration up to tens of PeV in the colliding flows during passage of the compact companion through the equatorial disk and rapid photomeson cooling allows for the interpretation of the very bright PeV photon flare detected by Carpet-2. Moreover, our mechanism unavoidably provides high neutrino flux, which could be detected by IceCube and other observatories.

ORCID iDs

A. M. Bykov https://orcid.org/0000-0003-0037-2288

A. E. Petrov https://orcid.org/0000-0001-8356-9654
M. E. Kalyashova https://orcid.org/0000-0002-8106-6567
S. V. Troitsky https://orcid.org/0000-0001-6917-6600

References

Aartsen, M. G., Abbasi, R., Abdou, Y., et al. 2013, PhRvL, 111, 021103
Aartsen, M. G., Ackermann, M., Adams, J., et al. 2019, ApJ, 886, 12
Abbasi, R., Ackermann, M., Adams, J., et al. 2021, PhRvD, 104, 022002
Abdalla, H., Aharonian, F., Ait Benkhali, F., et al. 2021, A&A, 653, A152
Abeysekara, A. U., Albert, A., Alfaro, R., et al. 2021, NatAs, 5, 465
Abeysekara, A. U., Benbow, W., Bird, R., et al. 2018, ApJL, 867, L19
Aharonian, F., Akhperjanian, A. G., Bazer-Bachi, A. R., et al. 2006, A&A, 460, 743
Aharonian, F., Yang, R., & de Oña Wilhelmi, E. 2019, NatAs, 3, 561
Albert, A., André, M., Anghinolfi, M., et al. 2018, ApJL, 868, L20
Amato, E. 2019, in PoS, High Energy Phenomena in Relativistic Outflows VII (Trieste: PoS), 33
Amenomori, M., Bao, Y. W., Bi, X. J., et al. 2021, PhRvL, 127, 031102
Arons, J. 2012, SSRv, 173, 341
Bednarek, W. 2005, ApJ, 631, 466
Bykov, A., Gehrels, N., Krawczynski, H., et al. 2012, SSRv, 173, 309
Bykov, A. M., Amato, E., Petrov, A. E., Krassilchtchikov, A. M., & Levenfish, K. P. 2017, SSRv, 207, 235
Bykov, A. M., Ellison, D. C., Gladilin, P. E., & Osipov, S. M. 2015, MNRAS, 453, 113
Camilo, F., Ray, P. S., Ransom, S. M., et al. 2009, ApJ, 705, 1
Cao, Z., Aharonian, F. A., An, Q., et al. 2021a, Natur, 594, 33
Cao, Z., Aharonian, F., An, Q., et al. 2021b, ApJL, 919, L22
Cerutti, B., Dubus, G., Malzac, J., et al. 2011, A&A, 529, A120
Chernyakova, M., Malyshev, D., Blay, P., van Soelen, B., & Tsygankov, S. 2020, MNRAS, 495, 365
Corbel, S., Dubus, G., Tomsick, J. A., et al. 2012, MNRAS, 421, 2947
Cristofari, P. 2021, Univ, 7, 324

Dermer, C. D., & Menon, G. 2009, High Energy Radiation from Black Holes: Gamma Rays, Cosmic Rays, and Neutrinos (Princeton, NJ: Princeton Univ. Press)
Distefano, C., Guetta, D., Waxman, E., & Levinson, A. 2002, ApJ, 575, 378
Dubus, G. 2013, A&ARv, 21, 64
Dzhappuev, D. D., Afashokov, Y. Z., Dzaparova, I. M., et al. 2021, ApJL, 916, L22
Falanga, M., Bykov, A. M., Li, Z., et al. 2021, A&A, 654, A127
HESS Collaboration, Abramowski, A., Aharonian, F., et al. 2016, Natur, 531, 476
Ho, W. C. G., Ng, C. Y., Lyne, A. G., et al. 2017, MNRAS, 464, 1211
IceCube Collaboration 2013, Sci, 342, 1242856
IceCube Collaboration 2020, GCN, 28927, 1
IceCube Collaboration, Abbasi, R., Ackermann, M., et al. 2021, ICRC (Berlin), 395, 1136
Kafexhiu, E., Aharonian, F., Taylor, A. M., & Vila, G. S. 2014, PhRvD, 90, 123014
Kelner, S. R., & Aharonian, F. A. 2008, PhRvD, 78, 034013
Kheirandish, A. 2020, Ap&SS, 365, 108
Klement, R., Carciofi, A. C., Rivinius, T., et al. 2017, A&A, 601, A74
Lemoine, M., & Waxman, E. 2009, JCAP, 2009, 009
Levinson, A., & Waxman, E. 2001, PhRvL, 87, 171101
Murase, K., & Fukugita, M. 2019, PhRvD, 99, 063012
Nikishov, A. 1962, Sov. Phys. JETP, 14, 393
Palladino, A., & Vissani, F. 2016, ApJ, 826, 185
Pittard, J. M., Romero, G. E., & Vila, G. S. 2021, MNRAS, 504, 4204
Romero, G. E., Boettcher, M., Markoff, S., & Tavecchio, F. 2017, SSRv, 207, 5
Sahakyan, N., Piano, G., & Tavani, M. 2014, ApJ, 780, 29
Shultz, M. E., Wade, G. A., Rivinius, T., et al. 2019, MNRAS, 490, 274
Sironi, L., Keshet, U., & Lemoine, M. 2015, SSRv, 191, 519
Takata, J., Tam, P. H. T., Ng, C. W., et al. 2017, ApJ, 836, 241
Tavani, M., & Arons, J. 1997, ApJ, 477, 439
Tibet ASγ Collaboration, Amenomori, M., Bao, Y. M., et al. 2021, NatAs, 5, 460